

# The absorption spectrum of the solvated electron in fluid helium by maximum entropy inversion of imaginary time correlation functions from path integral Monte Carlo simulations

E. Gallicchio<sup>a)</sup> and B. J. Berne

Department of Chemistry and Center of Biomolecular Simulations, Columbia University, New York, New York 10027

(Received 6 July 1994; accepted 23 August 1994)

The dipole absorption spectrum of an electron in fluid helium is calculated by the maximum entropy method (MEM) numerical inversion of quantum Monte Carlo data obtained from a path integral Monte Carlo (PIMC) simulation at 309 K at the reduced densities  $\rho^*=0.1, 0.3, 0.5, 0.7,$  and  $0.9$ . Our results agree with the RISM-polaron theory results of Nichols and Chandler [A. L. Nichols III and D. Chandler, *J. Chem. Phys.* **87**, 6671 (1987)] and the grid wave function calculation of Coker and Berne [D. F. Coker and B. J. Berne, *J. Chem. Phys.* **89**, 2128 (1988)]. The method generated the expected long high frequency tail and the low density zero-frequency intensity caused by high conductivity. The method has also been tested by comparing the MEM absorption spectrum to the analytical spectrum of an electron confined in a spherical cavity of fluctuating radius, a model for a solvated electron in a localized state. © 1994 American Institute of Physics.

## I. INTRODUCTION

The dipole spectral density function,  $I(\omega)$ , of a quantum system with Hamiltonian  $H$  with dipole operator  $\mu=\mu(x)$ , interacting with a classic monochromatic radiation of frequency  $\omega$ , is defined as<sup>1</sup>

$$I(\omega) = 2\pi \sum_{nn'} \frac{e^{-\beta E_n}}{Q} |\langle n | \mu | n' \rangle|^2 \delta[\omega - (E_{n'} - E_n)/\hbar], \quad (1)$$

where the inverse temperature is  $\beta=1/k_B T$  ( $k_B$  is the Boltzmann constant) and the sum is over all the pairs of the energy eigenstates  $|n\rangle$ . The energy of state  $|n\rangle$  is  $E_n$  and  $Q = \sum_n \exp(-\beta E_n)$  is the canonical partition function. The dipole spectral density function is the Fourier transform of the dipole-dipole autocorrelation function  $C(t)$ , namely

$$I(\omega) = \int_{-\infty}^{+\infty} dt e^{i\omega t} C(t), \quad (2)$$

where

$$\begin{aligned} C(t) &= \langle \mu(t) \mu(0) \rangle \\ &= \frac{\text{Tr}(e^{-\beta H} e^{itH/\hbar} \mu e^{-itH/\hbar} \mu)}{\text{Tr}(e^{-\beta H})} \\ &= \sum_{nn'} \frac{e^{-\beta E_n}}{Q} |\langle n | \mu | n' \rangle|^2 e^{-it(E_{n'} - E_n)/\hbar}. \end{aligned} \quad (3)$$

The coordinate representation of  $C(t)$ ,

$$C(t) = \frac{\int dx dx' \langle x | e^{-(\beta\hbar - it)H/\hbar} | x' \rangle \mu(x') \mu(x) \langle x' | e^{-itH/\hbar} | x \rangle}{\int dx \langle x | e^{-\beta H} | x \rangle}, \quad (4)$$

is the starting point for a path integral Monte Carlo calculation of the dipole correlation function which is, however, impractical even for simple systems because the method involves real time propagation with its attendant "wild" phase fluctuations.<sup>2</sup>

The imaginary (or Euclidean) time dipole autocorrelation function  $G(\tau)$  defined as  $G(\tau) = C(-i\tau)$ ,  $0 \leq \tau \leq \beta\hbar$ , contains the same physical information as the real time correlation function, being its analytic continuation on the imaginary axis.<sup>3</sup> The spectral density function  $I(\omega)$  and the imaginary time dipole autocorrelation function  $G(\tau)$  are a two-sided Laplace transform pair,

$$G(\tau) = \frac{1}{2\pi} \int_{-\infty}^{+\infty} d\omega I(\omega) e^{-\omega\tau}. \quad (5)$$

The calculation of  $G(\tau)$  can be tackled by standard quantum Monte Carlo techniques which are nowadays well developed and capable of simulating quite complex systems. However, the imaginary-time dipole autocorrelation function is rather insensitive to changes in the spectral density  $I(\omega)$ . Thus, for a reasonable uncertainty in  $G(\tau)$ , it is possible that two very different spectral densities functions  $I(\omega)$  can equally well give  $G(\tau)$  through the relation (5). Mathematically speaking the solution  $I(\omega)$  of the integral equation (5) is very unstable—small errors in  $G(\tau)$  produce large errors in  $I(\omega)$ .

In this paper we use the maximum entropy method (MEM),<sup>4</sup> which has proven to be reliable and efficient in similar ill-posed inversion problems,<sup>5,6</sup> to compute the dipole absorption spectrum of the solvated electron in fluid helium by numerical inversion of the integral equation (5) using the imaginary-time dipole autocorrelation function data obtained from a path integral Monte Carlo (PIMC) computer simulation.

We have tested the MEM inversion method by applying it to PIMC data obtained from the simulation of an electron in a spherical cavity of fluctuating radius, a model for a

<sup>a)</sup>In partial fulfillment of the Ph.D. in Chemical Physics at Columbia University.

solvated electron in a localized state. The calculated absorption spectrum has been compared with the available analytical solution and very good agreement has been found.

In the next section we review the theory and practice of the calculation of the imaginary-time dipole autocorrelation function by PIMC techniques. The application of MEM to the calculation of dipole spectral functions is presented in Sec. III. In Sec. IV we apply this numerical method to the calculation of the absorption spectrum of an electron in a spherical cavity of fluctuating radius. The absorption spectrum of a solvated electron in fluid helium by MEM inversion of an imaginary time correlation function, determined by a suitable PIMC computer simulation, is finally presented in Sec. V.

## II. PIMC CALCULATION OF THE IMAGINARY TIME DIPOLE CORRELATION FUNCTION

The canonical partition function in the coordinate representation

$$Q(\beta) = \text{Tr}(e^{-\beta H}) = \int dx \langle x | e^{-\beta H} | x \rangle \quad (6)$$

of a quantum system with Hamiltonian  $H$ , whose coordinates are described by the vector  $x$ , at the inverse temperature  $\beta$ , can be written, using the equality

$$e^{-\beta H} = [e^{-(\beta/p)H}]^p, \quad (7)$$

in the form

$$Q(\beta) = \int dx_1 \cdots dx_p \prod_{i=1}^p \langle x_i | e^{-(\beta/p)H} | x_{i+1} \rangle, \quad (8)$$

where  $x_{p+1} = x_1$ . In the particular case of a single particle at position  $\mathbf{r}$  in a potential  $V(\mathbf{r})$  and taking the usual free particle high temperature approximation

$$\begin{aligned} \langle \mathbf{r}_i | e^{-(\beta/p)H} | \mathbf{r}_{i+1} \rangle \\ \approx \left( \frac{\beta m \omega_p^2}{2\pi} \right)^{3/2} e^{-\beta [m \omega_p^2 (\mathbf{r}_i - \mathbf{r}_{i+1})^2 / 2 + V(\mathbf{r}_i) / p]}, \end{aligned} \quad (9)$$

where

$$\omega_p^2 = \frac{p}{(\beta \hbar)^2}, \quad (10)$$

we obtain the discretized path integral approximation to the canonical partition function<sup>7,8</sup>

$$\begin{aligned} Q(\beta) &\approx Q_p(\beta) \\ &= \left( \frac{\beta m \omega_p^2}{2\pi} \right)^{3p/2} \\ &\times \int d\mathbf{r}_1 \cdots d\mathbf{r}_p e^{-\beta \{ \sum_{i=1}^p [m \omega_p^2 / 2 (\mathbf{r}_i - \mathbf{r}_{i+1})^2 + V(\mathbf{r}_i) / p] \}}, \end{aligned} \quad (11)$$

which is isomorphic to the classical configurational partition function of a  $p$ -particle cyclic chain polymer in which the  $i$ th bead at position  $\mathbf{r}_i$  interacts with its neighbors through a harmonic bonds and with an external attenuated potential  $V(\mathbf{r})/p$ .<sup>9,10</sup>

The thermal average of some property  $O(\mathbf{r})$  can then be written as

$$\begin{aligned} \langle O \rangle &= \frac{1}{Q(\beta)} \text{Tr}(e^{-\beta H} O) \\ &\approx \frac{1}{Q_p(\beta)} \left( \frac{\beta m \omega_p^2}{2\pi} \right)^{3p/2} \int d\mathbf{r}_1 \cdots d\mathbf{r}_p \frac{1}{p} \\ &\times \sum_i O(\mathbf{r}_i) e^{-\beta \{ \sum_{i=1}^p [m \omega_p^2 (\mathbf{r}_i - \mathbf{r}_{i+1})^2 / 2 + V(\mathbf{r}_i) / p] \}}, \end{aligned} \quad (12)$$

which is equivalent to finding the average of some polymer property over all possible polymer configurations.

A useful correlation function, which gives information about the behavior of the quantum particle, is the mean-square displacement between pairs of points of the chain separated by the imaginary time increment  $\tau$  (Ref. 11),

$$R^2(\tau) = \langle [|\mathbf{r}(-i\tau') - \mathbf{r}[-i(\tau' + \tau)]|^2] \rangle \quad (13)$$

which is independent on the position of the first bead corresponding to the imaginary time  $\tau'$ . The  $R^2(\tau)$  correlation function is usually evaluated at the points  $\tau_j = \hbar \beta j / p$ ,  $j = 0, \dots, p/2$ , by the PIMC averages

$$R^2(\tau_j) = \langle \varrho_j \rangle, \quad (14)$$

where

$$\varrho_j = \frac{1}{p} \sum_{k=1}^p |\mathbf{r}_k - \mathbf{r}_{k+j}|^2, \quad j = 1, \dots, p/2. \quad (15)$$

The imaginary-time dipole autocorrelation function  $G(\tau)$  for the dipole operator  $\boldsymbol{\mu} = -|e|\mathbf{r}$ , where  $-|e|$  is the electron charge, is related to  $R^2(\tau)$  through

$$e^2 R^2(\tau) = 2[G(0) - G(\tau)]. \quad (16)$$

Using Eq. (5) and the detailed balance relation  $I(-\omega) = \exp(-\beta \hbar \omega) I(\omega)$ , we see that the spectral function (1) is related to  $R^2(\tau)$  through the integral equation

$$\begin{aligned} R^2(\tau) &= -\frac{1}{\pi e^2} \int_0^\infty d\omega I(\omega) [e^{-\omega\tau} + e^{-\omega(\beta\hbar - \tau)} \\ &\quad - (e^{-\beta\hbar\omega} + 1)]. \end{aligned} \quad (17)$$

The absorption cross section is defined as<sup>1</sup>

$$\sigma(\omega) = \frac{4\pi}{\hbar c} \omega (1 - e^{-\beta\hbar\omega}) I(\omega), \quad (18)$$

and is related to the imaginary-time  $R^2(\tau)$  correlation function through [see Eqs. (17) and (18)],

$$R^2(\tau) = -\frac{\hbar c}{4\pi^2 e^2} \int_0^\infty d\omega \sigma(\omega) \frac{\{\exp(-\omega\tau) + \exp[-\omega(\beta\hbar - \tau)] - \exp(-\hbar\omega\beta) - 1\}}{\omega [1 - \exp(-\beta\hbar\omega)]}. \quad (19)$$

The values of the  $R^2(\tau)$  correlation function at different values of  $\tau$  are not independent; instead, in the application presented, we have found a significant amount of cross correlation. This is best seen by the normalized cross-correlation matrix of the fluctuations  $\delta q_j = q_j - R^2(\tau_j)$ ,

$$\tilde{\mathcal{E}}_{ij} = \frac{\langle \delta q_i \delta q_j \rangle}{\sqrt{\langle \delta q_i^2 \rangle \langle \delta q_j^2 \rangle}} = \frac{\mathcal{E}_{ij}}{\sqrt{\mathcal{E}_{ii} \mathcal{E}_{jj}}}, \quad (20)$$

where

$$\mathcal{E}_{ij} = \langle \delta q_i \delta q_j \rangle / (L-1) \quad (21)$$

$q_j$  is defined in Eq. (15) and  $L$  is the number of samples.

The imaginary-time correlation function  $R^2(\tau)$  is determined only on the  $p$  discretization and its values are affected by statistical errors and biased due to approximations involved in the Monte Carlo simulation. There is, therefore, the need to resort to some method to obtain  $I(\omega)$  by numerical inversion of the integral equation (19) in such a way to bypass its intrinsic instability. Many standard methods fail in the present case because they amplify the errors on the Monte Carlo data and converge to solutions completely different from the exact one. The method we adopted, the maximum entropy inversion method, gives reasonable spectra in all test cases examined. The foundations of the method, presented briefly in the next section, are also well established increasing our confidence in applying it to nontrivial cases.

### III. THE MAXIMUM ENTROPY INVERSION METHOD

The maximum entropy inversion method<sup>12</sup> is applicable to the general problem of evaluating a set of unknowns from a data set knowing only the rule that generates the data from the unknowns, the inverse operation is never invoked and it can be assumed unavailable. We will focus on the numerical solution of the integral equation

$$D(\tau) = \int d\omega I(\omega) K(\omega, \tau), \quad (22)$$

where  $D(\tau)$  represents the calculated or measured data [in our case the imaginary-time dipole autocorrelation function  $G(\tau)$ ],  $I(\omega)$  is a positive unknown function and  $K(\omega, \tau)$  a regular kernel function. In practice  $D(\tau)$  is known only on a discrete set of points  $D_j = D(\tau_j)$ ,  $j = 1, \dots, M$ . To every  $D_j$  is also assigned an uncertainty  $\sigma_j$ . Analogously, we look for the values of  $I(\omega)$  on the set of points  $\omega_i$ ,  $i = 1, \dots, N$ , setting  $I_i = I(\omega_i) > 0$  and we carry out the integration in the finite interval  $\omega_{\min} \leq \omega \leq \omega_{\max}$ , implicitly assuming  $I(\omega) = 0$  outside this interval. We also assume that the data are uncorrelated, i.e., that the  $D_j$ 's can be considered independent variables. (See below for an illustration on how to apply MEM to correlated data once the correlation is known.)

The  $N$  unknowns  $\mathbf{I} = \{I_1, \dots, I_N\}$ , called hereafter the *map*, define a Cartesian  $N$ -dimensional space and the maximum entropy method assigns a probability distribution to  $\mathbf{I}$ , which is dependent on the data available, and defines the solution  $I(\omega)$  of Eq. (22) as the most probable map. Let  $\mathcal{P}(\mathbf{I}|\mathbf{D})$  be the probability of  $\mathbf{I}$  given the data  $\mathbf{D} = \{D_1, \dots, D_M\}$ . By Bayes theorem,

$$\mathcal{P}(\mathbf{I}|\mathbf{D}) \propto \mathcal{P}(\mathbf{I}) \mathcal{A}(\mathbf{D}|\mathbf{I}); \quad (23)$$

where  $\mathcal{P}(\mathbf{I})$  is the so called *prior* probability for  $\mathbf{I}$ , i.e., the probability distribution we assign to  $\mathbf{I}$  before acquiring the data, and  $\mathcal{A}(\mathbf{D}|\mathbf{I})$  is the *likelihood* probability, i.e., the probability of obtaining the data  $\mathbf{D}$  by the transformation (22) with the given map  $\mathbf{I}$ .

The prior distribution for the map is taken to be

$$\mathcal{P}(\mathbf{I}) \propto e^{\alpha S}, \quad (24)$$

where  $\alpha$  is an arbitrary positive parameter and  $S$  is the entropy function,

$$S = \sum_{i=1}^N \left( I_i - s_i - I_i \ln \frac{I_i}{s_i} \right), \quad (25)$$

whose unconstrained maximum occurs at  $I_i^* = s_i$  for which  $S^* = 0$ . The positive parameters  $s_i$  are chosen consistent with any prior information about the map that is available. If no prior information is available all the  $I_i$  have to be considered equivalent and, as we did in this work, the choice  $s_i = s = \text{constant}$  for every  $i$  has to be made. The form Eq. (25) for the entropy has been shown to be the only form consistent with the axioms of the MEM formalism.<sup>13</sup>

Now we turn to the problem of defining the likelihood probability distribution  $\mathcal{A}(\mathbf{D}|\mathbf{I})$ . In view of the necessary discretization described above, the integral transform Eq. (22) becomes a linear transformation  $\mathcal{K}$  from the  $N$ -dimensional map space to the  $M$ -dimensional data space. From a map  $\mathbf{I}$  we can, therefore, predict what the data ( $\mathcal{K}\mathbf{I}$ ) <sub>$j$</sub>  should be and get the residuals from the actual data given. If the residuals are not zero, and we exclude the possibility of systematic errors, it is because of statistical errors on the data. If we suppose the errors have Gaussian distributions described by standard deviations  $\sigma_j$ , we have

$$\mathcal{A}(\mathbf{D}|\mathbf{I}) \propto \prod_{j=1}^M \exp \left\{ - \frac{[D_j - (\mathcal{K}\mathbf{I})_j]^2}{2\sigma_j^2} \right\} \equiv \exp(-\chi^2/2). \quad (26)$$

Combining Eqs. (25) and (26) we see that the *posterior* probability whose maximum is the maximum entropy solution to the integral equation (22) is

$$\mathcal{P}(\mathbf{I}|\mathbf{D}) \propto \exp(\alpha S - \chi^2/2) \quad (27)$$

so that we are left with the problem of maximizing the function of  $N$  variables

$$Q(\mathbf{I}) = \alpha S(\mathbf{I}) - \chi^2(\mathbf{I})/2. \quad (28)$$

The arbitrary parameter  $\alpha$  is interpreted as the inverse Lagrange multiplier in the constrained maximization of  $S$  with a fixed value of  $\chi^2$ . If  $\alpha$  is large the maximum of  $Q(\mathbf{I})$  is mostly determined by the entropy function, i.e., by the prior information available. Thus, the MEM solution  $I(\omega)$  of the integral equation (22) [represented by the points  $(\omega_i, I_i)$ ] would be a smooth and flat function. If, instead,  $\alpha$  is small,  $I(\omega)$  is determined only by the  $\chi^2$  function, and it would then represent very well, in a  $\chi^2$  deviation sense, the data. It would also, however, represent any random error present in the data. Thus  $I(\omega)$  would be too sensitive to errors in the

data, would suffer high oscillations, and it would have little resemblance to the true solution of the integral equation. A common practice is to set  $\alpha$  so that, at the maximum of  $Q(\mathbf{I})$ ,  $\chi^2 = \text{number of observations} = M$  (which gives 99% confidence). More general criteria have been reported.<sup>14</sup>

In the present application, instead, we will regard  $\alpha$  as a regularization parameter that controls the degree of smoothness of the map  $\mathbf{I}$ . Regularization parameters are usually encountered in the theory of approximate solution of matrix equations  $Ax=b$  where the matrix of coefficients is ill-conditioned and many solutions  $x$  well represent the known vector  $b$ . In these cases the solution is usually chosen to be the best compromise between a good representation of the data  $b$  and some other criterion of regularization of the solution. Some of these regularization schemes are implemented in popular software packages for the numerical solution of ill-posed problems<sup>15</sup> where minimization of the norm of the solution and/or maximization of the degree of smoothness of the solution are used. Common to all these techniques is the problem of determining the best degree of regularization which in most cases depends, as in our case, on a single parameter. This is conveniently done using a graphical tool, the so-called *L-curve*.<sup>16,17</sup> In our case the regularization function is the entropy and the L-curve is a log-log plot, for all valid regularization parameters  $\alpha$ , of  $-S(I^*)$  vs the correspondent residual norm  $\chi^2(I^*)$  at the maximum of  $Q(\mathbf{I})$  in Eq. (28). For discrete ill-posed problems the L-curve has a characteristic L shape with a distinct corner separating the horizontal and vertical parts of the curve. The best value of  $\alpha$  corresponds to the corner, where the curvature of the L-curve is a maximum. At this point the best compromise between a minimum value for  $\chi^2$  and a maximum (i.e., less negative) value for the entropy is ensured.

The numerical problem of the constrained maximization of the entropy  $S$  has been solved even for very large  $N$  (a million or more points on the map) by very efficient algorithms<sup>18</sup> that have been applied successfully to the MEM reconstruction of 2D and 3D images with a large number of pixels. The present application is far less demanding in terms of dimensionality of the map space because a good representation of the spectral function is described, at most, by a few hundreds points. We are able, therefore, to use a safe but memory intensive Newton-Raphson based maximization procedure.<sup>19</sup> Moreover, the fact that  $\mathcal{H}$  in our case is linear ensures uniqueness of the maximum entropy solution.

In the maximum entropy inversion of the integral equation (19) from PIMC data we have  $D_j = R^2(\tau_j)$  and

$$\mathcal{H}_{ij} = -\frac{\hbar c}{4\pi^2 e^2} (\omega_{j+1} - \omega_j) \times \frac{[e^{-\omega_j \tau_i} + e^{-\omega_j(\beta\hbar - \tau_i)} - (e^{-\hbar\omega_j\beta} + 1)]}{\omega_j [1 - \exp(-\beta\hbar\omega_j)]} \quad (29)$$

derived from the discretization of the integral equation (19). As explained in Sec. II, the data  $R^2(\tau_j)$  cannot be considered independent. The  $\chi^2$  measure needed by the maximum entropy inversion algorithm in the case of correlated data is<sup>20</sup>

$$\chi^2 = \sum_{ij} [D_i - (\mathcal{H}\mathbf{I})_i] (\mathcal{E}^{-1})_{ij} [D_j - (\mathcal{H}\mathbf{I})_j], \quad (30)$$

where  $\mathcal{E}$  is the correlation matrix defined in Eq. (21). We also note that, if the positive definite, correlation matrix  $\mathcal{E}$  is properly diagonalized by an orthogonal matrix  $\mathcal{U}$ , the maximum entropy inversion of Eq. (19) can be carried out starting from the uncorrelated transformed data set  $\mathbf{D}' = \mathcal{U}^\dagger \mathbf{D}$  and the transformed linear relation from map space to data space  $\mathcal{H}' = \mathcal{U}^\dagger \mathcal{H}$ . The  $\sigma_j$ 's in Eq. (26) are, then, interpreted as the eigenvalues of the correlation matrix  $\mathcal{E}$ .

Our maximization algorithm maximizes the function  $Q(\mathbf{I})$  (28) with fixed  $\alpha$  using the Newton-Raphson method starting with the initial guess  $I_i = s_i = s$ ,  $i = 1, \dots, N$ , at the maximum of the entropy function (25) with a large value of  $\alpha$ . The intensity of the initial guess  $I_i = s$  is determined from the sum rule

$$R^2(\beta\hbar/2) = -s \frac{\hbar c}{4\pi^2 e^2} \int_0^\infty d\omega \times \frac{[2 \exp(\beta\hbar\omega/2) - \exp(-\beta\hbar\omega) - 1]}{\omega [1 - \exp(-\beta\hbar\omega)]}. \quad (31)$$

The inverse Lagrange multiplier  $\alpha$  is then progressively decreased until the maximum of curvature of the L-curve is reached. At every iteration convergence is checked by measuring the angle between the gradient of the entropy and the gradient of the  $\chi^2$  function. For the maximum entropy reconstructed spectra presented in this paper, the angle between the two gradients is less than  $1 \times 10^{-6}$  rad.

#### IV. TEST CASE: ELECTRON CONFINED IN A BREATHING SPHERICAL CAVITY

There are theoretical reasons<sup>13</sup> to believe that maximum entropy is the best and most flexible method to refine statistical data. In this section we test the performance of the maximum entropy method in reproducing the known exact absorption spectrum of an electron confined in a spherical cavity with variable radius by processing data obtained from an actual PIMC simulation. We have chosen this test case because the electron in a spherical cavity is a reasonable simplified model for a localized electron in a solvent. It constitutes, therefore, an appropriate benchmark problem to assess the reliability of MEM for the subsequent treatment the full microscopic model of the solvated electron.

The energy eigenfunctions in spherical polar coordinates for a particle of mass  $m_e$  in a spherical cavity of radius  $a$  are

$$\Psi_{nlm} = N_{nl} j_l(x_{nl}r/a) Y_{lm}(\theta, \varphi), \quad (32)$$

where  $[Y_{lm}(\theta, \varphi)]$  is a surface spherical harmonic,  $j_l(x)$  is the spherical Bessel function of order  $l$ ,  $x_{nl}$  its  $n$ th zero, and  $N_{nl}$  the appropriate normalization factor. The energy eigenvalues are given by

$$E_{nl} = \frac{\hbar^2}{m_e} \frac{x_{nl}^2}{2a^2} \quad (33)$$

and are  $(2l+1)$  fold degenerate. There are no restrictions on the values of  $l$  for a given  $n$ . The angular momentum states are labeled  $s, p, d, \dots$ , accordingly to common conventions ( $l = 1, 2, 3, \dots$ ).

The dipole line-spectrum at low enough temperature (or small enough radius) is determined by transitions originating from the ground state  $1s$ . The  $1s \rightarrow 1p$  line is the predominant feature of the spectrum, the transitions to higher  $p$  states being much less intense (the  $1s \rightarrow 2p$  transition is already 183 times less intense than the  $1s \rightarrow 1p$  transition and the transitions to states with angular momentum quantum number different from  $l=1$  are forbidden).

An inhomogeneously broadened spectrum can be obtained for an isobaric ensemble of spherical cavities containing one particle. In such a model only the radius of the sphere is allowed to fluctuate and the isobaric partition function  $\Delta$  at the external pressure  $P$  is given by

$$\Delta(\beta, P) = \int_0^\infty dV e^{-\beta PV} Q(\beta, V), \quad (34)$$

where  $Q(\beta, V)$  is the canonical partition function at the fixed radius  $a = (3/4\pi)^{1/3} V^{1/3}$ ,

$$Q(\beta, V) = \sum_{nl} (2l+1) \exp\left(-\beta \frac{\hbar^2 x_{nl}^2}{m_e 2a^2}\right). \quad (35)$$

In the following computations the pressure was adjusted to obtain an average sphere radius of 3–7 Å at room temperature corresponding to typical electron cavity sizes in various solvents. Under these conditions, the state of the electron is strongly ground state dominated ( $\beta\Delta E > 29$ ,  $\Delta E =$  energy of first excited state with respect to the ground state). It is, therefore, an excellent approximation to write

$$Q(\beta, V) = \exp\left[-\beta \frac{\hbar^2}{m_e} \left(\frac{4\pi}{3}\right)^{2/3} \frac{x_{1,0}^2}{2V^{2/3}}\right]. \quad (36)$$

Inserting Eq. (36) into Eq. (34) we see that the volume distribution function is

$$\mathcal{P}(V) = \Delta^{-1} \exp\left\{-\beta \left[ PV + \frac{\hbar^2}{m_e} \left(\frac{4\pi}{3}\right)^{2/3} \frac{x_{1,0}^2}{2V^{2/3}} \right]\right\}. \quad (37)$$

and, consequently, the radius distribution function is

$$\mathcal{P}(a) = \Delta^{-1} 4\pi a^2 \exp\left[-\beta \left( P \frac{4\pi}{3} a^3 + \frac{\hbar^2 x_{1,0}^2}{m_e 2a^2} \right)\right]. \quad (38)$$

Considering only the  $1s \rightarrow np$  transitions, the dipole spectral function at the fixed radius  $a$  is given by

$$I(\omega; a) = e^2 a^2 \sum_n v_n^2 \delta(\omega - \omega_n), \quad (39)$$

where

$$v_n = \frac{\int_0^1 dz z^2 J_{1/2}(x_{1,0}z) J_{3/2}(x_{n1}z)}{\sqrt{\int_0^1 dz z [J_{1/2}(x_{1,0}z)]^2} \sqrt{\int_0^1 dz z [J_{3/2}(x_{n1}z)]^2}}, \quad (40)$$

and

$$\omega_n = \frac{x_{n1}^2 - x_{1,0}^2}{2m_e a^2}. \quad (41)$$

We have taken the dipole operator to be  $-|e|\mathbf{r}$  and  $[J_l(x)]$  is the Bessel function of order  $l$ .

The inhomogeneously broadened spectrum is obtained by averaging the fixed radius spectrum over the radius distribution (38),

$$I(\omega) = \int_0^\infty da \mathcal{P}(a) I(\omega; a). \quad (42)$$

The expressions (39) and (42) define the analytical spectral density function, exact in the limit of complete ground state dominance, of an electron confined in the fluctuating-radius spherical cavity to which we compare the calculated spectrum.

We now address the problem of numerically obtaining the absorption cross section  $\sigma(\omega)$ , defined in Eq. (18), by a suitable Monte Carlo simulation, as described in Sec. II. The simulation yields the  $R^2(\tau)$  correlation function, defined in Eq. (14), which is then processed according to the maximum entropy recipe of Sec. III to solve the integral equation (19) for the desired absorption spectrum.

The  $R^2(\tau)$  correlation function of Eq. (14) for this system is given by PIMC averages over the volume of the spherical cavity and electron polymer configurations,

$$R^2(\tau_j) = \beta P \int_0^\infty dV e^{-\beta PV} \int d\mathbf{r}_1 \cdots d\mathbf{r}_p \times \left( \frac{1}{p} \sum_{k=1}^p |\mathbf{r}_k - \mathbf{r}_{k+j}|^2 \right) \prod_{i=1}^p G(\mathbf{r}_i, \mathbf{r}_{i+1}; \beta/p, a), \quad (43)$$

where

$$G(\mathbf{r}_i, \mathbf{r}_{i+1}; \beta/p, a) = \left( \frac{1}{2\pi\lambda_p^2} \right)^{3/2} \exp\left[ -\frac{(\mathbf{r}_i - \mathbf{r}_{i+1})^2}{2\lambda_p^2} \right] \times \left\{ 1 - \exp\left[ -\frac{2}{\lambda_p} (r_i - a)(r_{i+1} - a) \right] \right\} \quad (44)$$

is the spherical cavity image propagator<sup>21</sup> for the spherical radius  $a = (3/4\pi)^{1/3} V^{1/3}$ , and

$$\lambda_p = \sqrt{\frac{\beta\hbar^2}{pm_e}}. \quad (45)$$

The  $R^2(\tau)$  correlation function is symmetric around  $\beta\hbar/2$ . Thus, if  $p$  equally spaced discretization points are used, then there are at most  $p/2$  independent values of the correlation function  $R^2(\tau)$  available. Thus, in order to obtain numerous calculated points of the  $R^2(\tau)$  correlation function, we have found convenient to use the computationally inexpensive image propagator even though other proposed forms of the small  $\beta$  propagator are equally accurate for a smaller  $p$ .<sup>22</sup>

The MC sampling scheme consists in generating at every step a new free particle polymer configuration by the staging

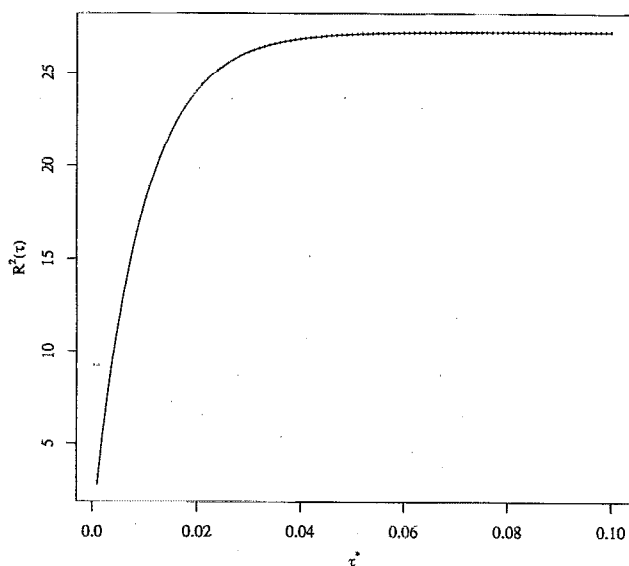


FIG. 1. Calculated  $R^2(\tau)$  correlation function of an electron in a breathing spherical cavity,  $\beta=1000$ ,  $p=1000$ , and  $P=5\times 10^{-5}$ . All values in atomic units,  $\tau^*=\pi\beta\hbar$ .

algorithm<sup>23</sup> followed by changing the volume of the cavity by a small step. The move is rejected or accepted, as in the usual Metropolis scheme, according to the ratio

$$\frac{e^{-\beta PV'}}{e^{-\beta PV}} \prod_{i=1}^p \frac{1 - \exp[-(2/\lambda_p^2)(r'_i - a')(r'_{i+1} - a')]}{1 - \exp[-(2/\lambda_p^2)(r_i - a)(r_{i+1} - a)]} \quad (46)$$

where the prime denotes a proposed new volume or new polymer configuration and the nonprimed variables denote the actual volume or configuration. The staging scheme and the volume step size are adjusted to obtain an average acceptance ratio of approximately 0.5.

The calculated  $R^2(\tau)$  correlation functions for  $\beta=1000$  a.u. (316 K),  $m_e=1$  a.u., and  $p=1000$  at the two pressures  $P=2\times 10^{-6}$  a.u. (581 atm) and  $P=5\times 10^{-5}$  a.u. (14 521 atm) after 80 000 Monte Carlo passes, are shown in Figs. 1 and 2.

We find that the cavity radius distribution functions generated by the MC sampling scheme deviate only slightly from the analytical ones [Eq. (38)]. The calculated average cavity radius is 3.675 Å (analytical 3.665 Å) with a standard deviation of 0.113 Å (analytical 0.112 Å) for the high pressure case and 7.082 Å (analytical 7.027 Å) with a standard deviation of 0.415 Å (analytical 0.406 Å) for the low pressure case.

The first and last rows of the cross correlation matrix [Eq. (20)] corresponding to the correlation of the first (last) point on the  $R^2(\tau)$  function with respect to all the other points are shown in Fig. 3 for the low pressure case. Similar results for the cross correlation are obtained for the high pressure case.

The maximum entropy reconstructions of the dipole absorption spectra, using the method developed in the previous sections, are shown in Figs. 4 and 5, compared with the

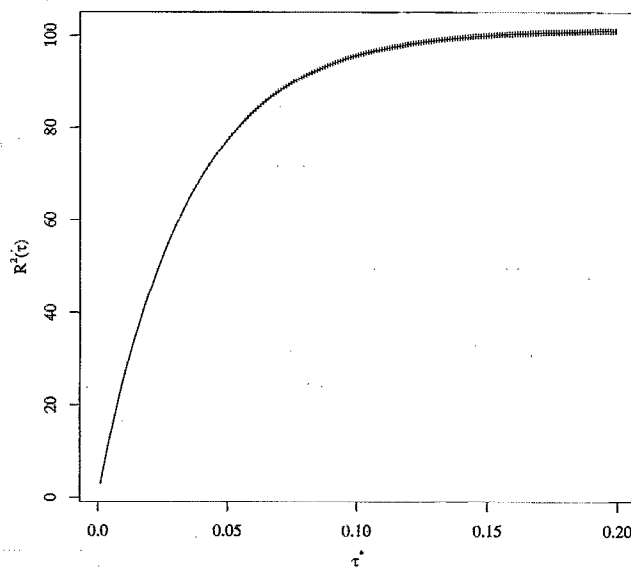


FIG. 2. Calculated  $R^2(\tau)$  correlation function of an electron in a breathing spherical cavity,  $\beta=1000$ ,  $p=1000$ , and  $P=2\times 10^{-6}$ . All values in atomic units,  $\tau^*=\pi\beta\hbar$ .

analytical ones from Eqs. (42) and (18). The analytical calculation used the radius distribution obtained from the simulations to focus on errors in the spectrum due only to the maximum entropy inversion. It can be observed that, in the range of frequencies examined, only two peaks are observed; the larger one is the  $1s \rightarrow 1p$  transition, and the smaller one, barely discernible from the base line, corresponds to the

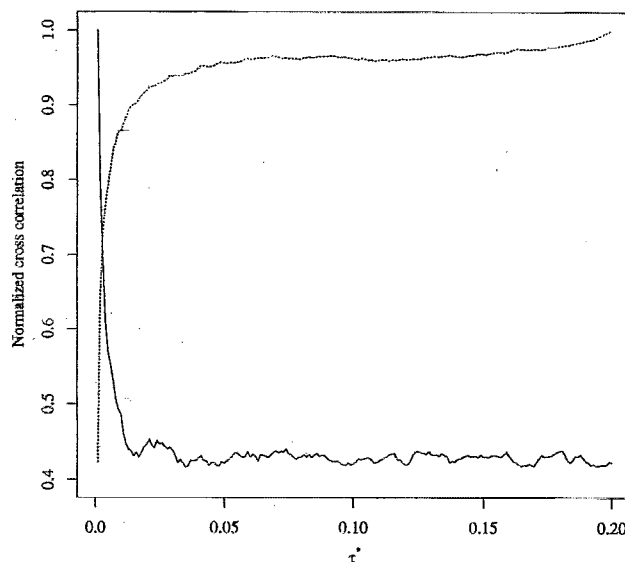


FIG. 3. Two rows of the normalized cross correlation matrix  $\mathcal{S}$  [see Eq. (20)], as a function of  $j$  for  $i=1$  (full line) and  $i=200$  (broken line), for an electron in a breathing spherical cavity. The relation between the discrete indexes and the imaginary time is  $\tau_j = \beta\hbar j/p$ ,  $\beta=1000$ ,  $p=1000$ , and  $P=2\times 10^{-6}$ . All values in atomic units,  $\tau^*=\pi\beta\hbar$ .

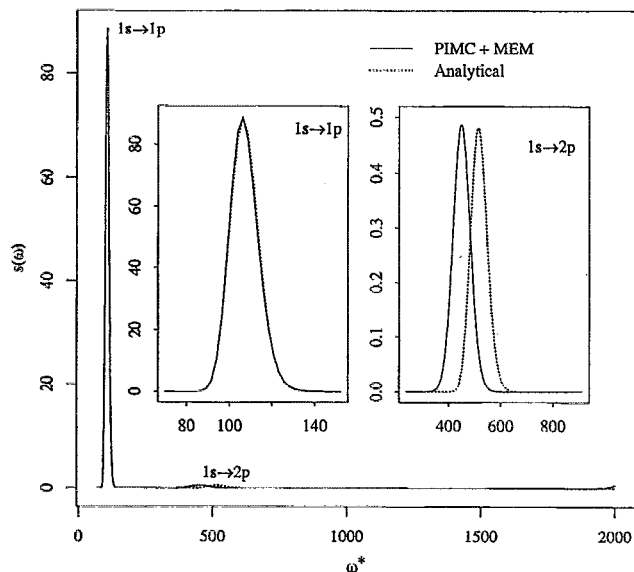


FIG. 4. Dipole absorption spectrum of an electron in a breathing spherical cavity from maximum entropy inversion of PIMC data,  $\beta=1000$ ,  $p=1000$ ,  $P=5 \times 10^{-5}$ ,  $\omega^* = \beta \hbar \omega$ , and  $s(\omega) = \hbar c \sigma(\omega) / 8 \pi^2 e^2$ . The analytical spectrum and enlargements of the peaks are also shown. All values in atomic units.

$1s \rightarrow 2p$  transition. The fact that the simulated correlation functions  $R^2(\tau)$  are extremely insensitive to the detailed structure in the spectral function and that there is a large intensity difference between the two peaks suggest that a good reconstruction of the spectrum will be difficult to obtain. Nevertheless, we notice that the MEM reconstructions

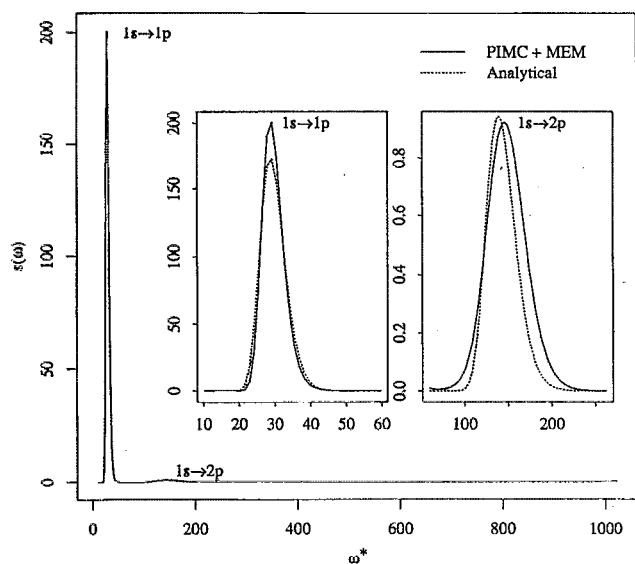


FIG. 5. Dipole absorption spectrum of an electron in a breathing spherical cavity from maximum entropy inversion of PIMC data,  $\beta=1000$ ,  $p=1000$ ,  $P=2 \times 10^{-6}$ ,  $\omega^* = \beta \hbar \omega$ , and  $s(\omega) = \hbar c \sigma(\omega) / 8 \pi^2 e^2$ . The analytical spectrum and enlargements of the peaks are also shown. All values in atomic units.

well reproduce the main features of the spectra. Only the reconstruction of the  $1s \rightarrow 2p$  peak in the high pressure spectrum is somewhat red shifted with respect to the exact one but the peak shape is well preserved. In an attempt to improve the agreement, reasoning that at this pressure the average radius of the cavity is roughly half of the low pressure case and the stronger interaction of the polymer with the cavity walls would require a finer path integral discretization, we ran a simulation with a number of polymer beads twice as large ( $p=2000$ ) but the resulting  $1s \rightarrow 2p$  peak (not shown) showed a blue shift of similar amount with respect to the exact peak position.

A spurious structure (very small in the scale of Fig. 5) is present at the right end limit of the frequency range of both spectra that indicates a residual intensity at larger frequencies not contained in the frequency range examined. As expected, the intensity of the structure increases when considering a smaller frequency range. If the frequency window is set to leave out the  $1s \rightarrow 2p$  peak but wide enough to contain the tail of the  $1s \rightarrow 1p$  peak, the intensity at the right edge becomes quite large but the accuracy of the reconstruction of the  $1s \rightarrow 1p$  peak is unaffected or even improves. It seems, therefore, that a single strong peak is easier to reconstruct than a spectrum composed of two peaks of very different intensity. This is an important characteristic of the maximum entropy reconstructed spectra because in the localized solvated electron case only one, wider, peak is expected and, in view of these observations, it should be easy to obtain through MEM inversion of PIMC data.

## V. THE OPTICAL ABSORPTION OF A SOLVATED ELECTRON IN FLUID HELIUM

The PIMC formulation of a single quantum particle interacting with a fixed external potential is described in Sec. II. In the case of an electron interacting with a classical solvent, PIMC samples solvent configurations weighted by the appropriate Boltzmann factor. The canonical average of a property  $O(\mathbf{r}, \mathbf{R}^M)$  of the mixed quantum-classical system is

$$\langle O \rangle = \frac{1}{Q_p(\beta)} \left( \frac{\beta m \omega_p^2}{2\pi} \right)^{3p/2} \int d\mathbf{R}^M e^{-\beta \Phi(\mathbf{R}^M)} \int d\mathbf{r}_1 \cdots d\mathbf{r}_p \frac{1}{p} \times \sum_i O(\mathbf{r}_i, \mathbf{R}^M) e^{-\beta \{ \sum_i [(m\omega_p^2/2)(\mathbf{r}_i - \mathbf{r}_{i+1})^2 + V(\mathbf{r}_i, \mathbf{R}^M)/p] \}}, \quad (47)$$

where  $\mathbf{r}_i$  are the coordinates of the electron beads and  $\mathbf{R}^M$  describes the  $M$ -degrees of freedom configuration of the solvent. The canonical partition function is

$$Q_p(\beta) = \left( \frac{\beta m \omega_p^2}{2\pi} \right)^{3p/2} \int d\mathbf{R}^M e^{-\beta \Phi(\mathbf{R}^M)} \times \int d\mathbf{r}_1 \cdots d\mathbf{r}_p e^{-\beta \{ \sum_i [(m\omega_p^2/2)(\mathbf{r}_i - \mathbf{r}_{i+1})^2 + V(\mathbf{r}_i, \mathbf{R}^M)/p] \}}, \quad (48)$$

where  $\Phi(\mathbf{R}^M)$  is the interaction potential between solvent molecules and  $V(\mathbf{r}, \mathbf{R}^M)$  is the interaction potential between solvent molecules and the electron.<sup>24</sup>

The classical helium fluid was modeled via Lennard-Jones 12-6 pair potential where  $\sigma=2.556 \text{ \AA}$  and  $\epsilon=10.22 \text{ K}$ . The electron-solvent interaction was modeled through a pair pseudopotential between electron beads and solvent atoms. The form of the electron-atom pseudopotential is

$$V(r) = \frac{A}{r^4} \left( \frac{B}{C+r^6} - 1 \right), \quad (49)$$

where, for helium,  $A=16\,220 \text{ \AA}^4 \text{ K}$ ,  $B=1956.5 \text{ \AA}^6$ , and  $C=276.86 \text{ \AA}^6$ .<sup>25</sup>

The Monte Carlo sampling of the electron-helium system was performed by sequentially selecting solvent atoms and moving each by a random displacement, calculating the solvent-solvent and electron-solvent energy change associated with the move and accepting or rejecting according to the standard Metropolis scheme. After having cycled through all the solvent atoms, a new electron polymer configuration is generated by the staging method,<sup>26</sup> taking into account the external potential due to the solvent atoms, until each electron bead is displaced. The solvent atom step size and the staging scheme are adjusted to obtain an average acceptance ratio of approximately 0.5. After every Monte Carlo cycle the quantity  $\varrho_j$ ,  $j=1, \dots, p/2$  defined in Eq. (15), whose average is  $R^2(\tau_j)$ , is accumulated and stored. The normalized cross-correlation matrix [Eq. (20)] is calculated at the end of the simulation by block-averaging.<sup>27</sup>

The electron-helium system has been studied at the temperature  $T=309 \text{ K}$  at the reduced fluid densities  $\rho^*=\rho\sigma^3=0.1, 0.3, 0.5, 0.7,$  and  $0.9$  using a periodic cubic simulation box with 864 helium atoms and 1000 electron beads. The calculated  $R^2(\tau)$  correlation functions after 20 000 MC passes, found to be in agreement with previous simulations,<sup>25</sup> are shown in Fig. 6. In order to minimize computer time spent to accumulate the values of the correlation functions, the number of calculated points of the  $R^2(\tau)$  correlation functions has been reduced by ignoring the less informative plateau portion. When a plateau could not be identified, not all points allowed by the number of beads on the electron polymer have been considered in the calculation. The number of calculated points on the  $R^2(\tau)$  correlation functions ranges from 200 to 250. The calculated cross correlation matrices  $\mathcal{C}_{ij}$  showed, especially at low fluid densities, less correlation between different points of the  $R^2(\tau)$  correlation functions than the ones found in Sec. IV for the electron in a breathing spherical cavity.

The absorption cross sections  $\sigma(\omega)$  defined in Eq. (18) at the fluid densities considered have been evaluated by the maximum entropy procedure described in the previous section and are shown in Fig. 7. Figure 7 shows only the lower frequency portion of the full frequency range used; in the computations the upper limit of the frequency interval was increased until the spurious intensity at the upper limit (also observed in the absorption spectra calculations of the electron in a breathing sphere) became negligible small. The number of MC passes in the PIMC calculation of the  $R^2(\tau)$  correlation functions was also increased until the maximum entropy generated spectra did not show important changes.

All the spectra, except for the lowest density spectrum, are composed of a single peak and of a long high frequency

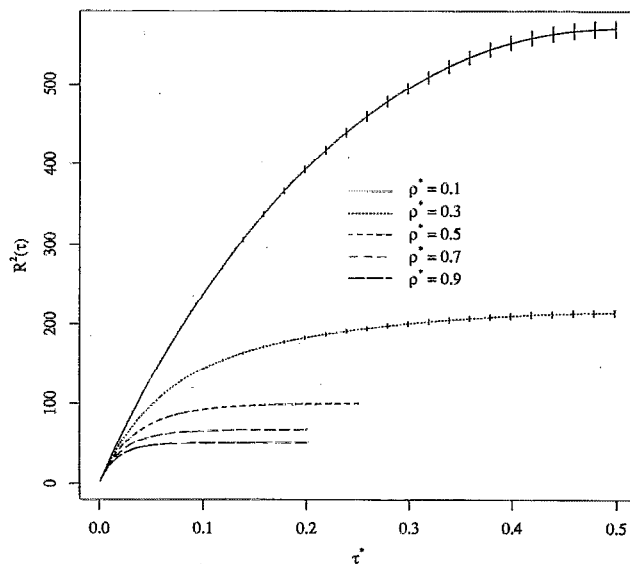


FIG. 6. Calculated  $R^2(\tau)$  correlation functions in atomic units of a single electron in fluid helium at 309 K ( $\beta=1021 \text{ a.u.}$ ) at several reduced densities. Error bars are shown every 10 calculated points;  $\tau^* = \pi\beta\hbar$ .

tail. The position of the peaks is in agreement with the findings of Coker and Berne<sup>28</sup> who calculated the transition dipole moments from the electron's ground state to the first excited states and averaged over a limited number of fluid configurations generated by a PIMC simulation. The spectra presented in this paper differ substantially from the ones of Coker and Berne in which the high frequency tail is absent. They found that their spectra missed nearly 40% of the total

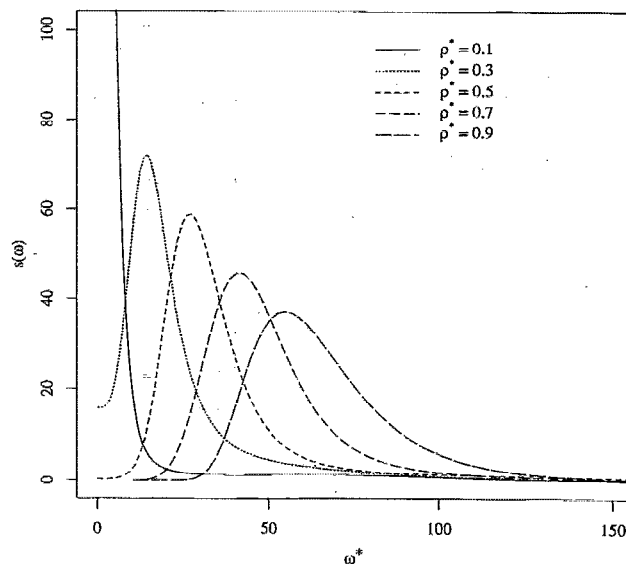


FIG. 7. Dipole absorption spectrum in atomic units of a single electron in fluid helium at 309 K ( $\beta=1021 \text{ a.u.}$ ) at several reduced densities from maximum entropy inversion of PIMC data;  $\omega^* = \beta\hbar\omega$ ,  $s(\omega) = \hbar c \sigma(\omega) / 8\pi^2 e^2$ .

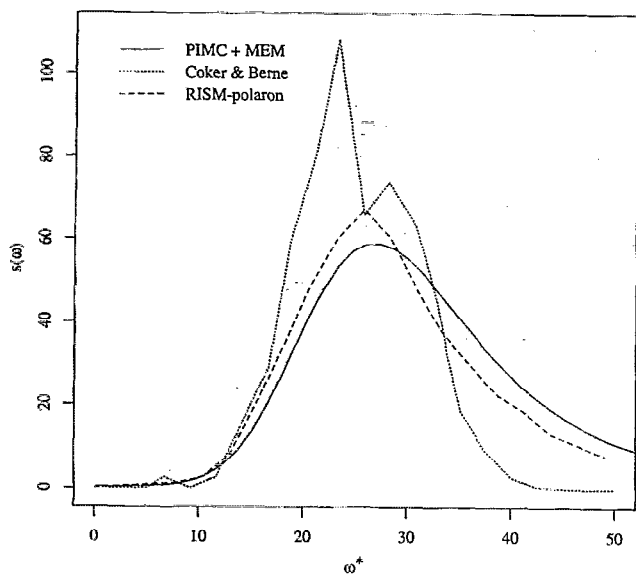


FIG. 8. Dipole absorption spectrum in atomic units of a single electron in fluid helium at 309 K ( $\beta=1021$  a.u.) at the reduced density  $\rho^*=0.5$ . "PIMC + MEM" is this work. The wave function calculation data ("Coker and Berne") and the RISM-polaron theory are both taken from Ref. 28.  $\omega^*=\beta\hbar\omega$ ,  $s(\omega)=\hbar c\sigma(\omega)/8\pi^2 e^2$ .

oscillator strength because the technique they used only consider a small range of energy states in the continuum. Because we are using a correlation function method to evaluate the spectra, we are treating both the continuum and the localized states equally well. We believe, therefore, that the observed tail is due to transitions from the ground state to excited states in the continuum while the peak itself is ascribed to transitions from the ground state of type  $s$  to the localized first excited states of type  $p$ . At the lowest fluid density considered no peak is observed but only a tail that shows that, at this density, the spectrum is dominated by extended states. A similar behavior for the absorption spectra has been predicted by the RISM-polaron theory of Chandler *et al.*<sup>29,30</sup> In particular, the observed nonzero intensity at  $\omega=0$  for the spectra at the two lowest densities is an indication of large conductivity of the fluid due to the high electron mobility found at these densities.

The MEM reconstructed absorption cross section of the solvated electron in fluid helium at  $\rho^*=0.5$  is compared in Fig. 8 with the simulation results of Coker and Berne<sup>28</sup> and the RISM-polaron theory results for the associated hard sphere model of Nichols and Chandler.<sup>30</sup> We see that the computations performed here are in good agreement with the analytical predictions of the RISM-polaron theory.

Apart from the comparisons presented with previous approximate calculations, we cannot directly test the accuracy of the spectra presented since experimental measurements are not available and an exact analytical treatment of this system is not known. There are two possible source of errors: (i) systematic and statistical errors on the PIMC data due to the finiteness of the path-integral imaginary time discretization and the finiteness of the simulation run and (ii) errors

introduced on the spectra by the maximum entropy inversion procedure.

The statistical errors are fully treated by the MEM method as explained in Sec. III and in the limit of zero statistical error the MEM reconstruction reproduces the exact spectra compatible with the  $R^2(\tau)$  correlation function. Our data are, of course, affected by statistical errors but we have been careful to run sufficiently long simulations so that the spectra reached convergence. We can therefore rule out such a source of errors as an important one, especially for the high density cases where statistical errors are minute.

Systematic errors due to the finite number ( $p=1000$ ) of electron beads are more important at high densities where the solvent cage is smaller and the electron-solvent interactions more intense. We have found in the previous section for the electron confined in a spherical breathing cavity that, only in the high pressure case, such errors caused a red shift of the very weak  $1s \rightarrow 2p$  peak. (see Figs. 4 and 5) but the main peak position and shape were well reproduced. We are confident, therefore, that the value of  $p$  we used in the electron-helium simulations is sufficient even at the highest density. At this density, the solvent cage is roughly twice as large as in the high pressure case of the of the spherical breathing cavity.

We believe that errors introduced by the MEM numerical inversion on the absorption spectra presented here can be considered negligible in view of the fact that, for an electron in the breathing spherical cavity, this procedure is able to resolve spectral bands of quite different intensities and narrow spectral widths—a rather strenuous test case. In this paper we have used the MEM method with an *ad hoc* procedure to select the parameter  $\alpha$  [cf. Eq. (28)]; by using selection methods which are self-consistently generated by the maximum entropy formalism,<sup>14</sup> it should be possible to determine the absorption spectra with greater accuracy and by implementing other extensions of the MEM method<sup>5</sup> it should also be possible to estimate the errors introduced by the MEM inversion.

In conclusion, we are confident that the absorption spectra of the solvated electron in fluid helium presented here are a good representation of the exact ones.

## ACKNOWLEDGMENTS

We are grateful to Dr. Joel Bader, Dr. Steve Rick, and Dr. Tom Pollard for their helpful comments on several aspects of this work. This work was supported by a grant from the NSF (NSF CHE-91-22-506).

<sup>1</sup> B. J. Berne, in *Physical Chemistry, an Advanced Treatise*, edited by H. Eyring (Academic, New York, 1967-75), Vol. VIII B, Chap. 9.

<sup>2</sup> D. Thirumalai and B. J. Berne, *Comput. Phys. Commun.* **63**, 415 (1991).

<sup>3</sup> G. Baym and D. Mermin, *J. Math. Phys.* **2**, 232 (1960).

<sup>4</sup> *Maximum Entropy in Action*, edited by J. Skilling (Kluwer Academic, New York, 1989).

<sup>5</sup> R. N. Silver, D. S. Sivia, and J. E. Gubernatis, *Phys. Rev. B* **41**, 2380 (1990); J. E. Gubernatis, M. Jarrell, R. N. Silver, and D. S. Sivia, *Phys. Rev. B* **44**, 6011 (1991).

<sup>6</sup> K. Livesey, P. Licinio, and M. Delays, *J. Chem. Phys.* **84**, 5102 (1986).

<sup>7</sup> R. P. Feynman and A. R. Hibbs, *Quantum Mechanics and Path Integrals* (McGraw-Hill, New York, 1965).

- <sup>8</sup>R. P. Feynman, *Statistical Mechanics* (Addison-Wesley, Reading, MA, 1972).
- <sup>9</sup>D. Chandler and P. G. Wolynes, *J. Chem. Phys.* **74**, 4078 (1981).
- <sup>10</sup>B. J. Berne and D. Thirumalai, *Annu. Rev. Phys. Chem.* **37**, 401 (1986).
- <sup>11</sup>D. Chandler, in *Liquids, Freezing and Glass Transition*, edited by D. Levesque, J. P. Hansen, and J. Zinn-Justin (Elsevier, New York, 1990).
- <sup>12</sup>J. Skilling, in *Maximum Entropy in Action*, edited by J. Skilling (Kluwer Academic, Dordrecht, 1989).
- <sup>13</sup>J. Skilling, in *Maximum Entropy and Bayesian Methods*, edited by J. Skilling (Kluwer Academic, Dordrecht, 1989).
- <sup>14</sup>S. F. Gull, in *Maximum Entropy and Bayesian Methods*, edited by J. Skilling (Kluwer Academic, Dordrecht, 1989).
- <sup>15</sup>P. C. Hansen, *Regularization Tools. A Matlab Package for Analysis and Solution of Discrete Ill-Posed Problems* (Danish Computing Center for Research and Education, 1992), revised 1993. This report and the software therein described is available via Netlib (netlib.att.com) from the directory NUMERALGO.
- <sup>16</sup>C. L. Lawson and R. J. Hanson, *Solving Least Square Problems* (Prentice-Hall, Englewood Cliffs, NJ, 1974).
- <sup>17</sup>K. Miller, *SIAM J. Math. Anal.* **1**, 52 (1970).
- <sup>18</sup>J. Skilling and R. K. Bryan, *Mon. Not. R. Astron. Soc.* **211**, 111 (1984).
- <sup>19</sup>D. A. Pierre, *Optimization Theory with Applications* (Dover, New York, 1986).
- <sup>20</sup>R. N. Silver, J. E. Gubernatis, and D. S. Sivia, *Phys. Rev. Lett.* **65**, 496 (1990).
- <sup>21</sup>J. A. Barker, *J. Chem. Phys.* **70**, 2914 (1979).
- <sup>22</sup>J. Cao and B. J. Berne, *J. Chem. Phys.* **97**, 2382 (1992).
- <sup>23</sup>M. Sprick, M. L. Klein, and D. Chandler, *Phys. Rev. B* **31**, 4234 (1985).
- <sup>24</sup>D. F. Coker and B. J. Berne, in *Excess Electrons in Dielectric Media*, edited by Jean-Paul Jay-Gerlin and C. Ferradini (Chemical Rubber, Boca Raton, 1991).
- <sup>25</sup>D. F. Coker, B. J. Berne, and D. Thirumalai, *J. Chem. Phys.* **86**, 5689 (1987).
- <sup>26</sup>M. E. Tuckerman, B. J. Berne, G. J. Martyna, and M. L. Klein, *J. Chem. Phys.* **99**, 2796 (1993).
- <sup>27</sup>M. P. Allen and D. J. Tildesley, *Computer Simulations of Liquids* (Clarendon, Oxford, 1987).
- <sup>28</sup>D. F. Coker and B. J. Berne, *J. Chem. Phys.* **89**, 2128 (1988).
- <sup>29</sup>D. Chandler, Y. Singh, and D. M. Richardson, *J. Chem. Phys.* **81**, 1975 (1984).
- <sup>30</sup>A. L. Nichols III and D. Chandler, *J. Chem. Phys.* **87**, 6671 (1987).